Electronic Supplementary Material (ESI) for Journal of Materials Chemistry C.


# Precise, Sensitive, and Reversible Thermochromic Luminescent Sensing Facilitated *via* Bright High-Temperature Luminescent $PEAMnBr_xI_{3-x}$ (x = 0/1/2/3)

Wei Shen [a,b,*,‡], Shiqi Sui [a,‡], Wenbo Yuan [c], Aifei Wang [a], Youtian Tao [c], Shufen Chen [b,*] and Zhengtao Deng [a,*]

[a] Department of Biomedical Engineering, College of Engineering and Applied Sciences, Nanjing National Laboratory of Microstructures, Collaborative Innovation Center of Chemistry for Life Sciences, Nanjing University, Nanjing, Jiangsu 210093, P. R. China.

[b] Key Laboratory for Organic Electronics and Information Displays & Jiangsu Key Laboratory for Biosensors, Institute of Advanced Materials (IAM), Jiangsu National Synergetic Innovation Center for Advanced Materials (SICAM), Nanjing University of Posts & Telecommunications (NUPT), 9 Wenyuan Road, Nanjing 210023, P. R. China.

[c] Key Lab for Flexible Electronics & Institute of Advanced Materials (IAM), Nanjing Tech University, 30 South Puzhu Road, Nanjing 211816, P. R. China.

## Experimental Section

### Materials

$MnBr_2$ (99.9%, Strem Chemicals), $Mn_2CO_3$ (99.95%, Aladdin), β-phenethylamine (98%, Aladdin), HBr (48%, Macklin), HI (55% - 58%, with ≤ 1.5% $H_3PO_2$, Aladdin), ethyl ether (≥ 99.5%, Sinopharm Chemical Reagent Co., Ltd.), ethyl acetate (≥ 99.5%, Sinopharm Chemical Reagent Co., Ltd.).

### Characterization

Steady state absorbance spectra were collected with a Shimadzu UV-3600 plus spectrophotometer equipped with an integrating sphere under ambient conditions. The high scanning rate model was used with 0.1 s integration and 20 nm slit width. The luminescence spectra were collected with Thorlabs CCS-175 compact CCD spectrometers with corresponding fiber bundles under ambient-condition operating. Wavelength of exciting laser was 385 nm and integration time was 1000 ms. Photoluminescence quantum yield data were collected with a Horiba PTI QuantaMaster 400 steady-state fluorescence system. Powder samples were measured in corresponding integrating sphere under 385 nm excitation. Slits width was 0.8 nm. Steps size was 0.5 nm. Integration time was 0.2 s. Temperature-dependent X-ray diffractions spectra were collected with a Bruker D8 ADVANCE X-ray Powder Diffractometer equipped a Cu Kα. Measurement range was from 5° to 50°. Step size was 0.0195°. Temperature range was from 30 °C to 120 °C. Luminescence lifetime were fitted according to fluorescence decay curves which were collected with an Edinburgh FLS-980 steady-state fluorescence spectrometers. Curve-fitting algorithm and calculation were based on Origin 2018 program. Powder samples were measured in quartz micro-cells. X-ray photoelectron spectra were collected with a PHI 5000 VersaProbe from UlVAC-PHI Company. Scanning electron microscope photos were collected with a Zeiss ULTRA 55 Scanning Electron Microscope system. Energy dispersive X-ray spectra were collected with an Oxford Inca X-MAX EDS accessory equipped on SEM. Thermogravimetric data were collected with a PerkinElmer TGA 8000 system. Samples were measured from 30 °C to 150 °C under $N_2$ atmosphere. Differential scanning calorimetry data were collected with a PerkinElmer Pyris 1 DSC system. Samples were measured from 60 °C to 150 °C under $N_2$ atmosphere.

### Preparation of $MnI_2$

$MnI_2$ was prepared by reaction of $MnCO_3$ and HI. Briefly, 1.15 g (10 mmol) $MnCO_3$ powder was added into a 100 mL beaker with 50 mL ethanol under ice bath. Then 15 mmol HI solution was injected dropwise into the beaker with vigorous stirring. After 2 h, a clear solution was obtained and $MnI_2$ powder was prepared *via* freeze-drying of solution.

### Preparation of PEABr and PEAI

PEABr was prepared by reaction of PEA and HBr. Briefly, 10 mmol PEA was added into a 100 mL beaker with 50 mL ethanol. Then 15 mmol HBr was injected dropwise into the solution under ice bath. Precipitate occurred rapidly under vigorously stirring. After 2 h, the solution changed into light yellow fluid. White powder was obtained by extraction filtration. Recrystallization was used to purify the product with ethanol as solvent. Final crystal was washed by ethyl ether. PEAI was prepared by similar process, except 15 mmol HBr was replaced by 15 mmol HI.

### Synthesis of $PEAMnBr_xI_{3-x}$ (x = 0/1/2/3)

$PEAMnBr_xI_{3-x}$ (x = 0/1/2/3) was synthesized by PEAX and MnX2 (X = Br / I). Briefly, 0.5 mmol PEAX and 0.5 mmol $MnX_2$ were dissolved into 5 mL ethyl acetate via ultrasonic. The solution was heated to 150 °C for crystallization. $PEAMnBr_3$ was synthesized by 0.5 mmol PEABr and 0.5 mmol $MnBr_2$. $PEAMnBr_2I$ was synthesized by 0.5 mmol PEAI and 0.5 mmol $MnBr_2$. $PEAMnBrI_2$ was synthesized by 0.5 mmol PEABr and 0.5 mmol $MnI_2$. $PEAMnI_3$ was synthesized by 0.5 mmol PEAI and 0.5 mmol $MnI_2$.

***Additional Supporting Figures:***

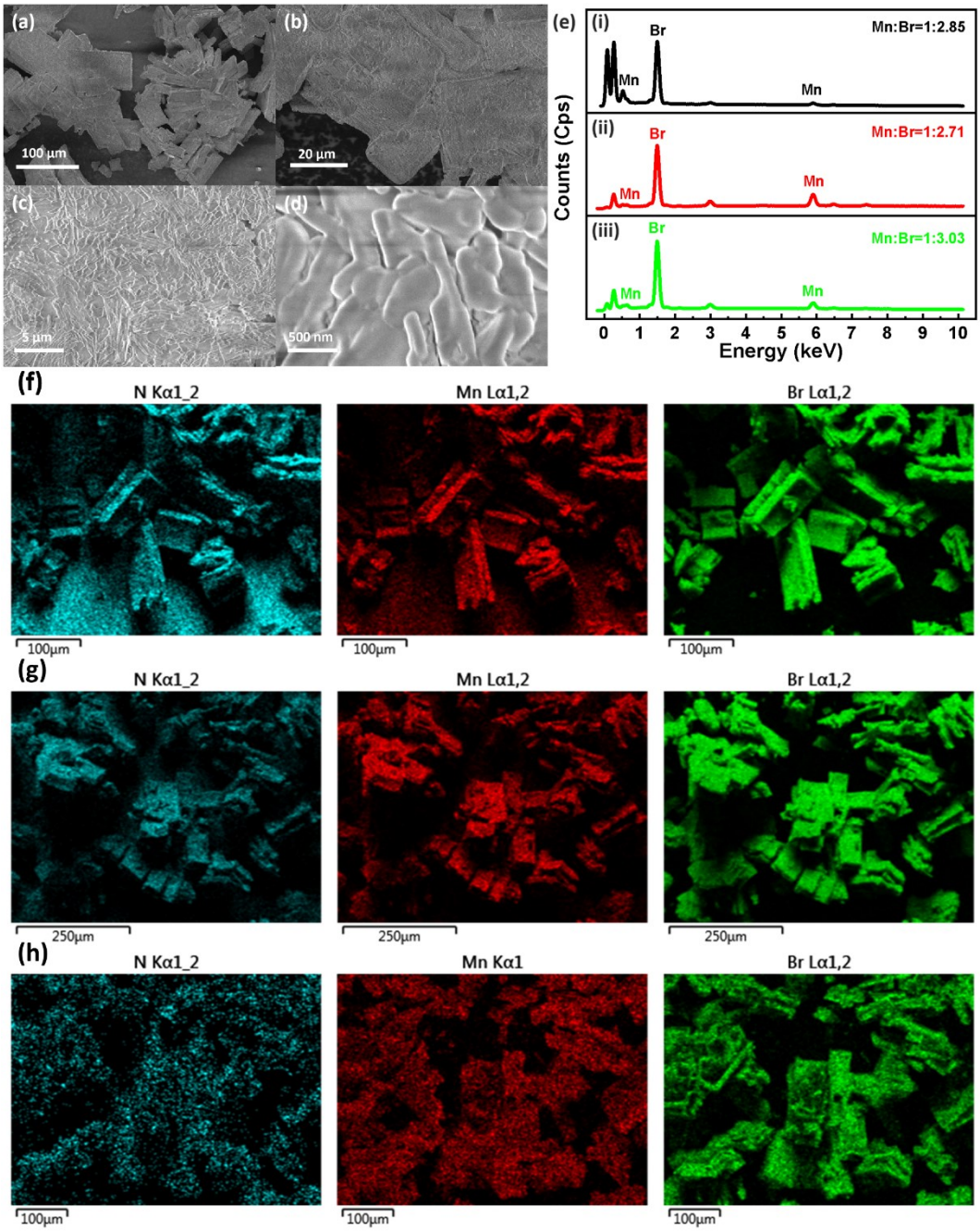


**Figure S1.** (a-d) SEM images of $PEAMnBr_3$. (e) EDS spectra at 3 random locations of $PEAMnBr_3$. (f-h) Element mappings of $PEAMnBr_3$ corresponding to (e). (Figure S1f correspond to Figure S1e-i; Figure S1g correspond to Figure S1e-ii, Figure S1h correspond to Figure S1e-iii).

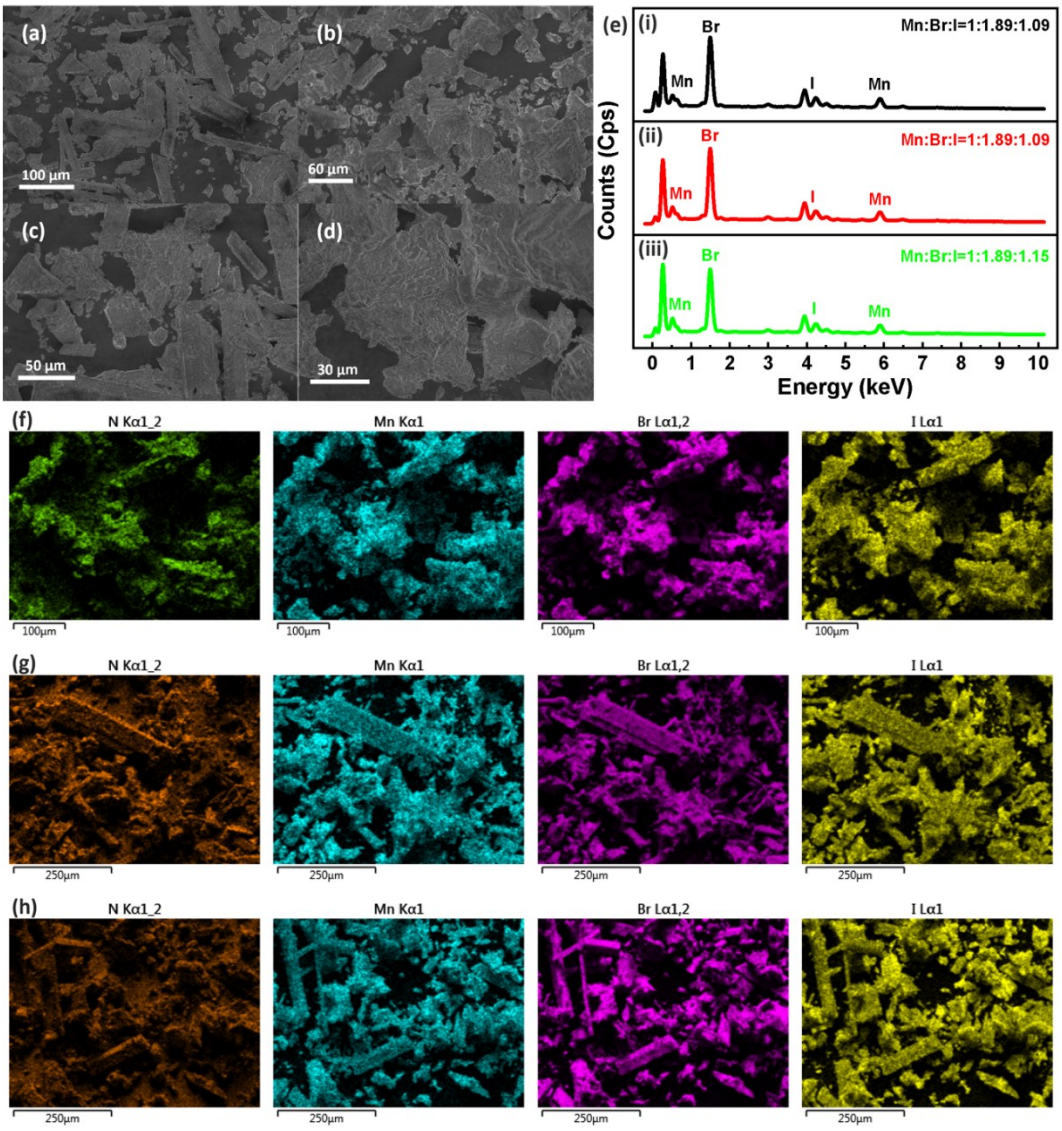


**Figure S2.** (a-d) SEM images of $PEAMnBr_2I$. (e) EDS spectra at 3 random locations of $PEAMnBr_2I$. (f-h) Element mappings of $PEAMnBr_2I$ corresponding to (e). (Figure S2f correspond to Figure S2e-i; Figure S2g correspond to Figure S2e-ii, Figure S2h correspond to Figure S2e-iii).

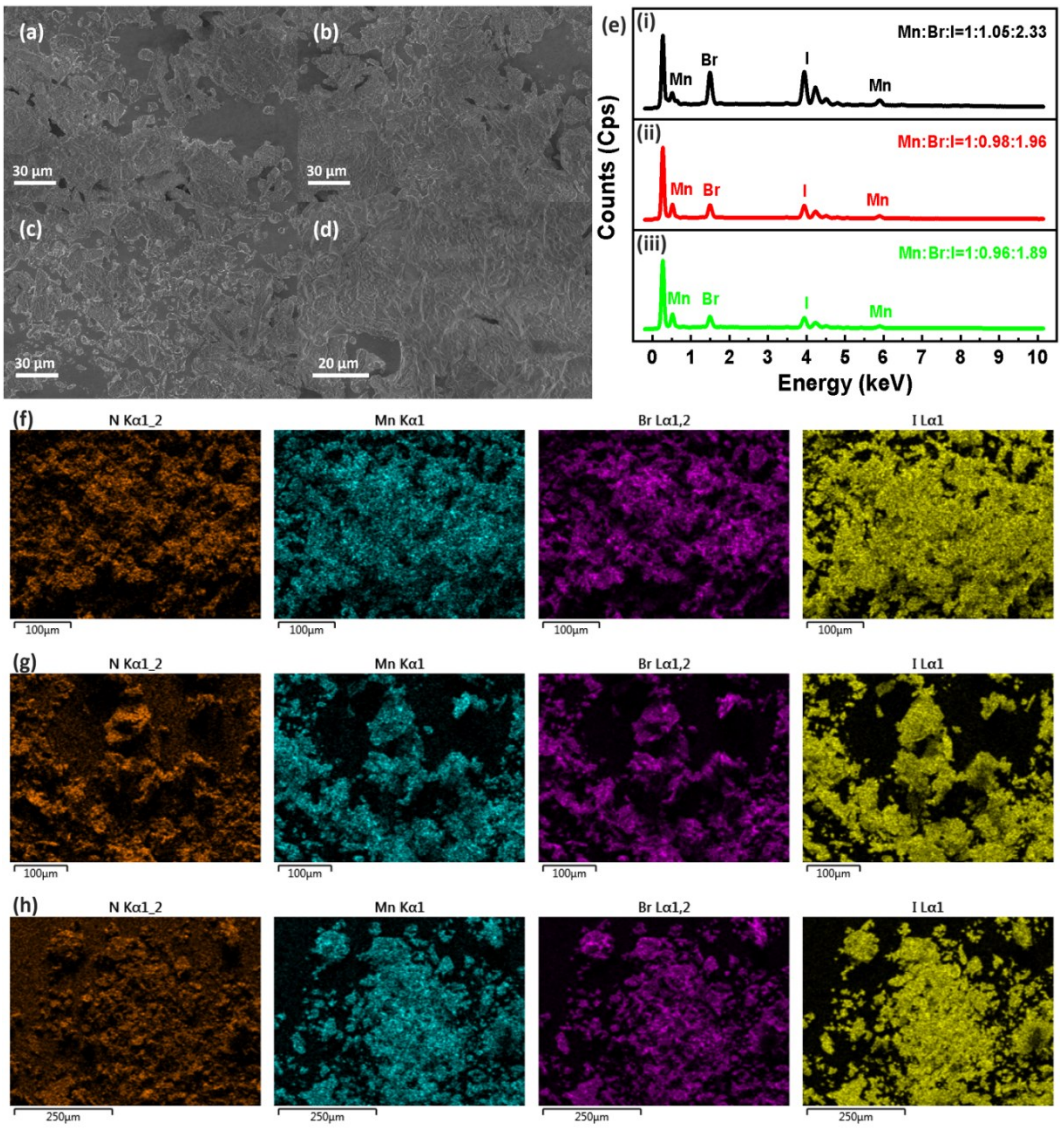


**Figure S3.** (a-d) SEM images of $PEAMnBrI_2$. (e) EDS spectra at 3 random locations of $PEAMnBrI_2$. (f-h) Element mappings of $PEAMnBrI_2$ corresponding to (e). (Figure S3f correspond to Figure S3e-i; Figure S3g correspond to Figure S3e-ii, Figure S3h correspond to Figure S3e-iii).

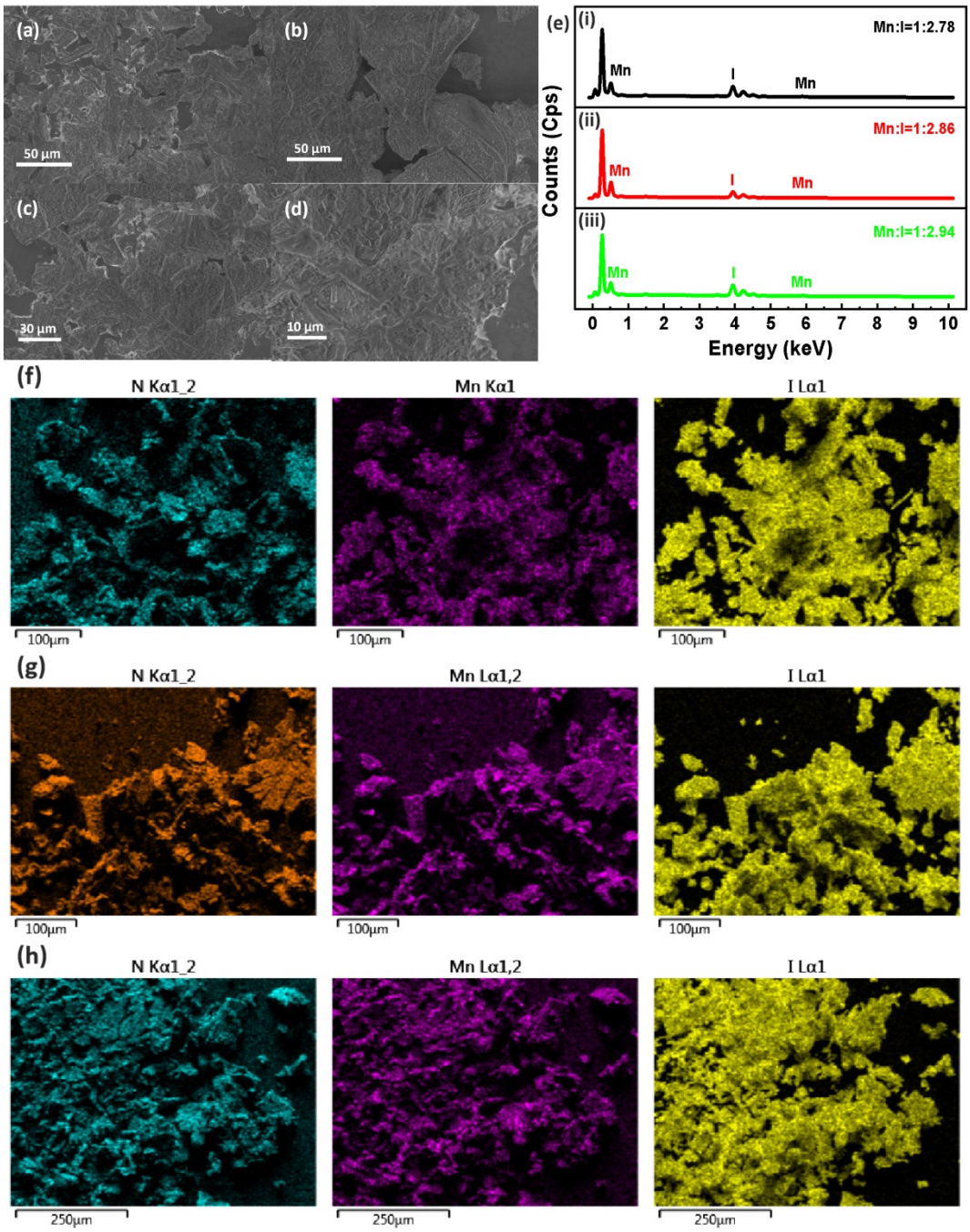


**Figure S4.** (a-d) SEM images of $PEAMnI_3$. (e) EDS spectra at 3 random locations of $PEAMnI_3$. (f-h) Element mappings of $PEAMnI_3$ corresponding to (e). (Figure S4f correspond to Figure S4e-i; Figure S4g correspond to Figure S4e-ii, Figure S4h correspond to Figure S4e-iii).

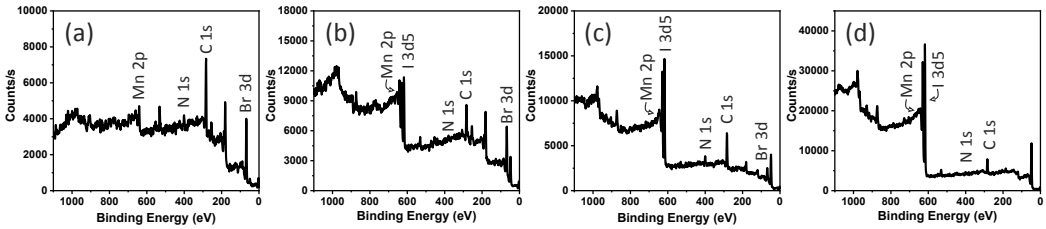


**Figure S5.** XPS spectra of $PEAMnBr_xI_{3-x}$ (a: x = 3; b: x = 2; c: x = 1; d: x=0).

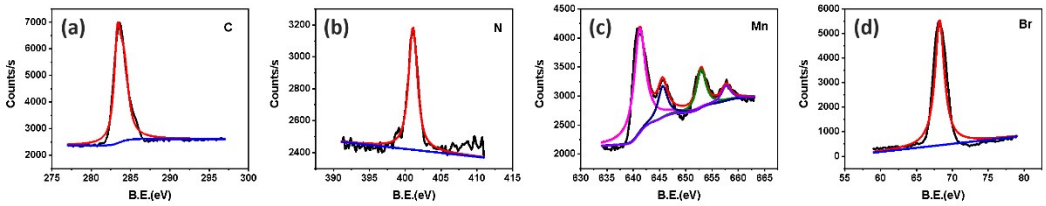


**Figure S6.** XPS fine spectra of different elements of $PEAMnBr_3$ (a: C; b: N; c: Mn; d: Br). Elements contents were obtained *via* calculation of peak integration.

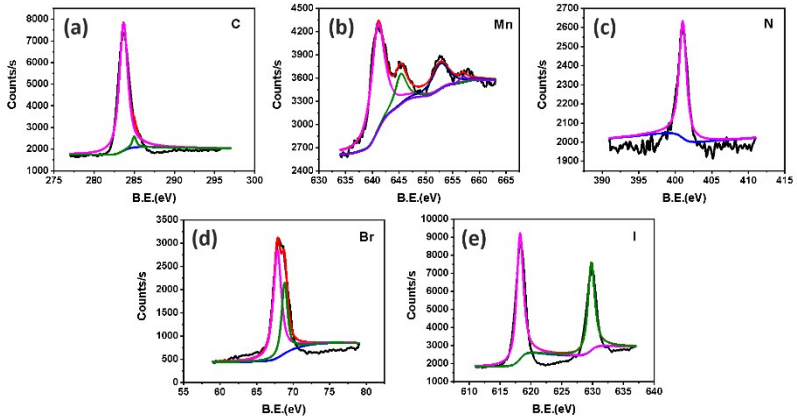


**Figure S7.** XPS fine spectra of different elements of $PEAMnBr_2I$ (a: C; b: N; c: Mn; d: Br; e: I). Elements contents were obtained *via* calculation of peak integration.

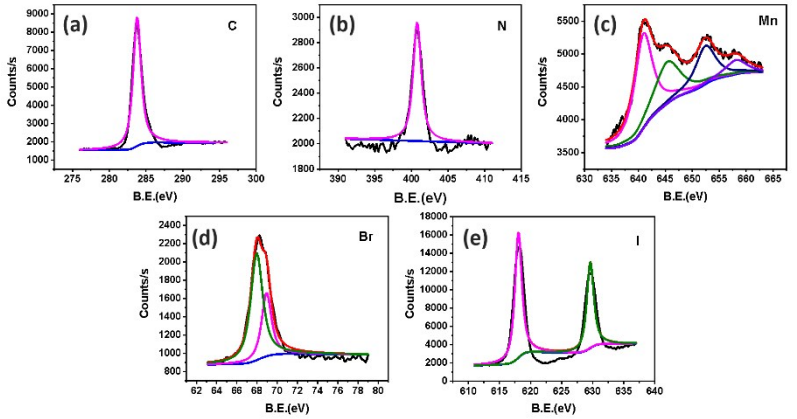


**Figure S8.** XPS fine spectra of different elements of $PEAMnBrI_2$ (a: C; b: N; c: Mn; d: Br; e: I). Elements contents were obtained *via* calculation of peak integration.

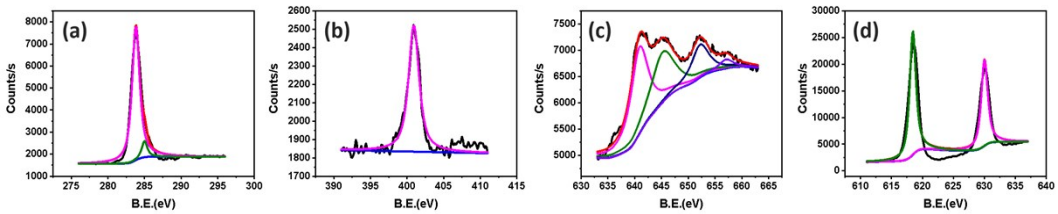


**Figure S9.** XPS fine spectra of different elements of $PEAMnI_3$ (a: C; b: N; c: Mn; d: I). Elements contents were obtained *via* calculation of peak integration.

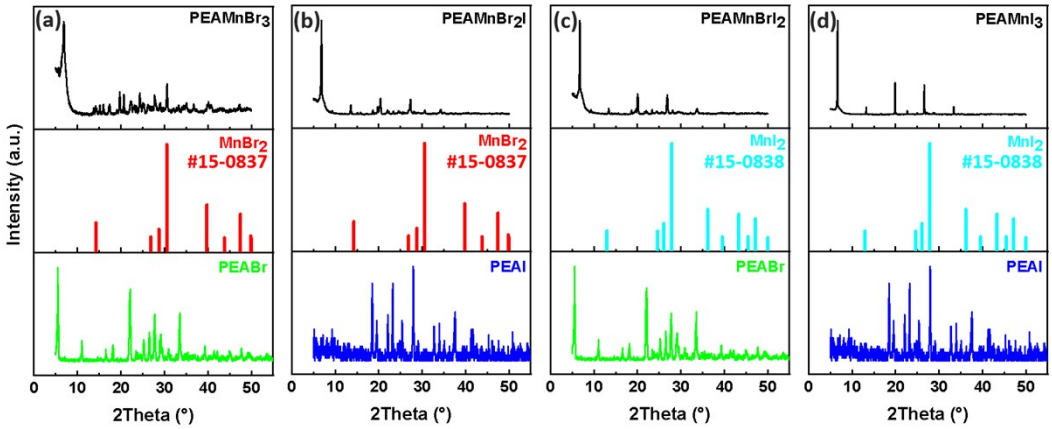


**Figure S10.** XRD patterns contrast between raw materials and products. a: $PEAMnBr_3$, $MnBr_2$ and PEABr. b: $PEAMnBr_2I$, $MnBr_2$ and PEAI. c: $PEAMnBrI_2$, $MnI_2$ and PEABr. d: $PEAMnI_3$, $MnI_2$ and PEAI. Obviously, new peaks indicated formation of $PEAMnBr_xI_{3-x}$ (x = 0/1/2/3).

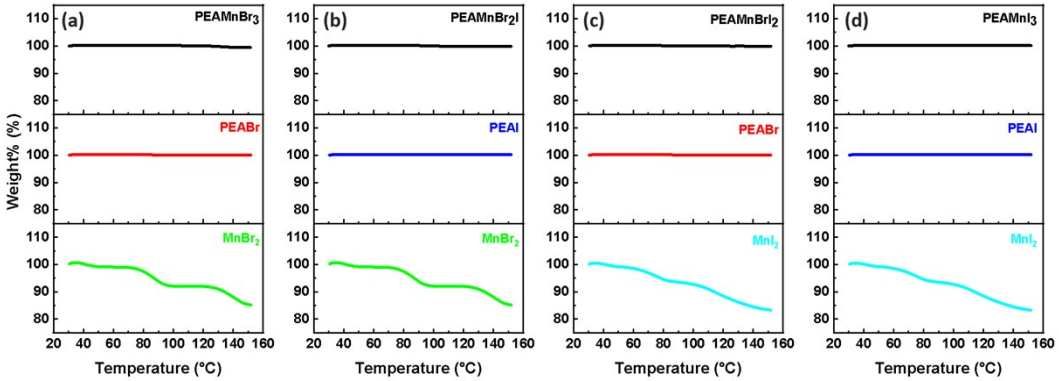


**Figure S11.** TGA curves contrast between raw materials and products. a: $PEAMnBr_3$, $MnBr_2$ and PEABr. b: $PEAMnBr_2I$, $MnBr_2$ and PEAI. c: $PEAMnBrI_2$, $MnI_2$ and PEABr. d: $PEAMnI_3$, $MnI_2$ and PEAI. The weight of PEABr and PEAI would not change during temperature elevation, whereas the weight of $MnBr_2$ and $MnI_2$ decreased due to the loss of water. The weights of $PEAMnBr_xI_{3-x}$ (x = 0/1/2/3) were kept the same, which indicated the raw materials were completely converted to $PEAMnBr_xI_{3-x}$ (x = 0/1/2/3).

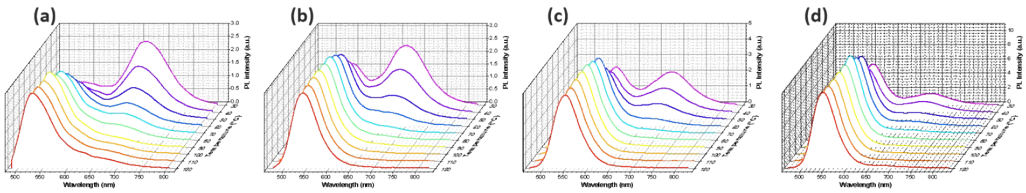


**Figure S12.** Temperature dependent luminescence spectra of $PEAMnBr_xI_{3-x}$ (a: x = 3; b: x = 2; c: x = 1; d: x=0).

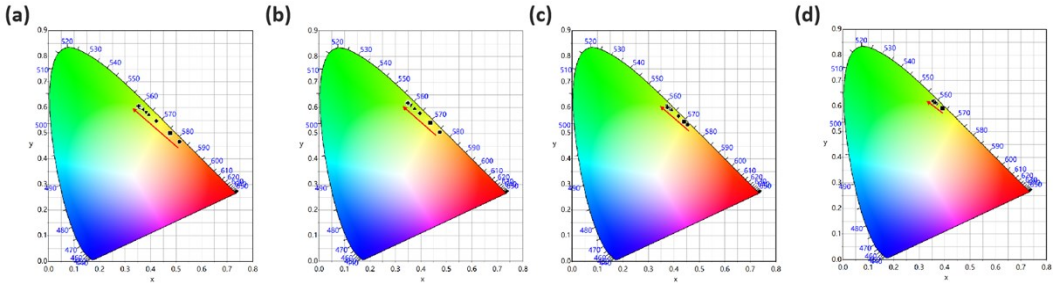


**Figure S13.** CIE figures of $PEAMnBr_xI_{3-x}$ (a: x = 3; b: x = 2; c: x = 1; d: x=0). The arrows showed the color coordinates changing with increasing temperature from 30 °C to 120 °C.

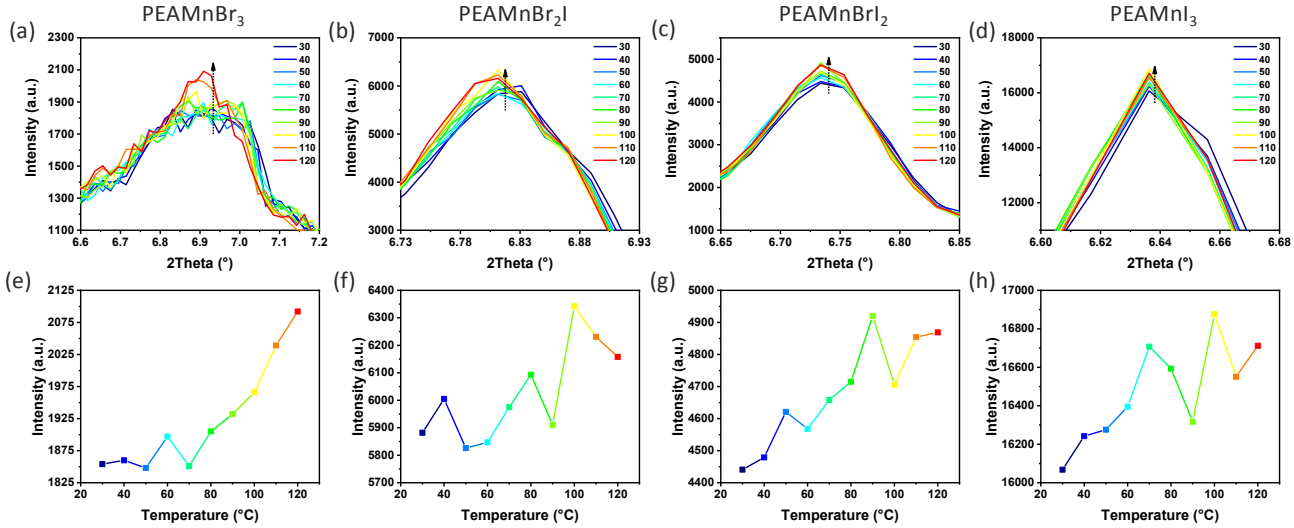


**Figure S14.** (a-d) Detailed XRD patterns in the range of 27° to 32°. Patterns in different temperature were marked by different colour. The increasement of peak intensity were marked by a dot-line arrow. (e-h) Line chart of the growth trend according to the corresponding intensity from (a-d). Intensities at different temperature were marked by different colour.

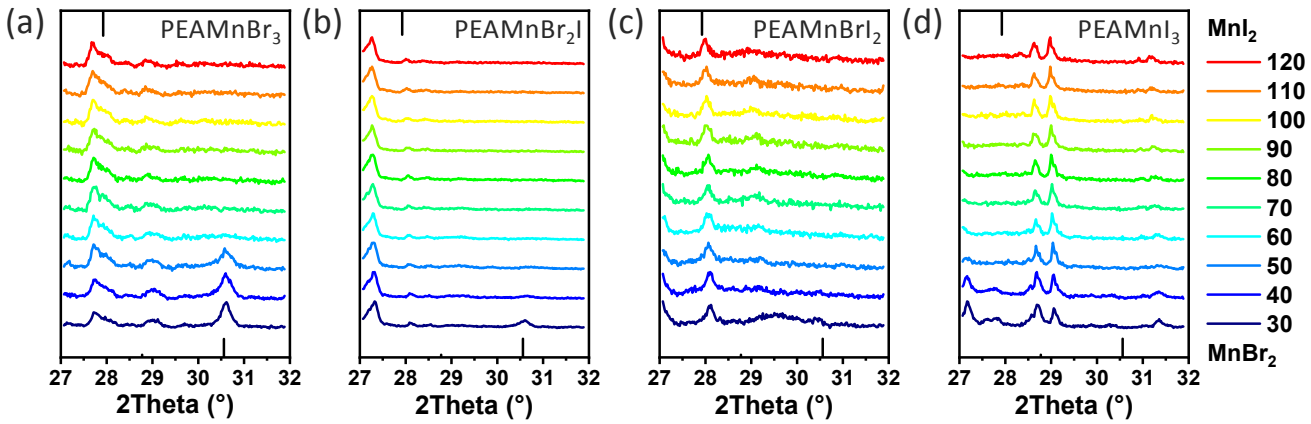


**Figure S15.** Detailed XRD patterns in the range of 27° to 32°. Patterns in different temperature were marked by different colour which were listed at the right. The standard diffraction peaks were marked with the black lines and the corresponding composition were listed in the right.

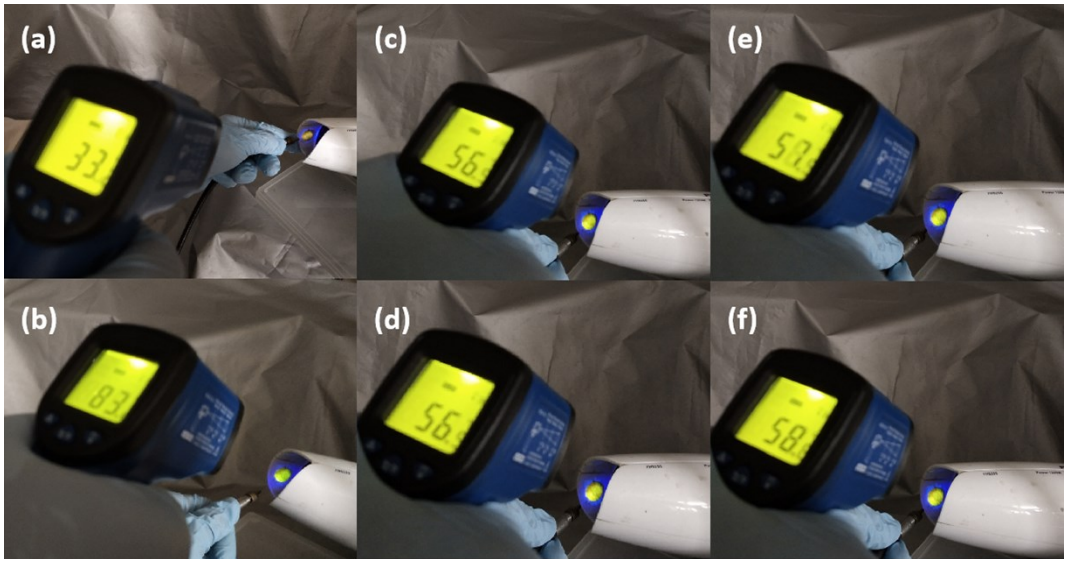


**Figure S16.** Photos of polymer films with $PEAMnBr_2I$ in different temperature. The films were excited by 385 nm excitation laser, and their spectra were collected by fiber bundles of Thorlabs CCS-175 compact CCD spectrometers. (a). Luminescence photo under room temperature. IR thermometer result was 33.9 °C. (b). Luminescence photo under high temperature. IR thermometer result was 83.3 °C. (c-f). Luminescence photos in the conditions of 56.9 °C, 57.5 °C, 56.5 °C and 58.3 °C according to IR thermometer results, separately.

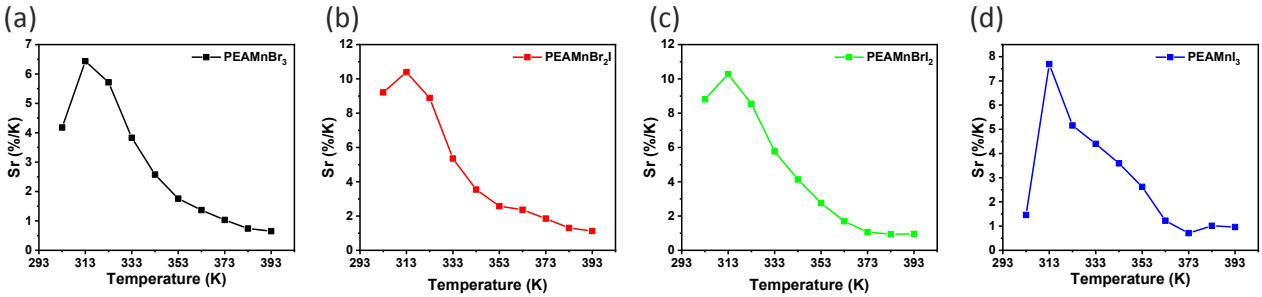


**Figure S17.** Temperature dependence of the relative sensitivity values for $PEAMnBr_xI_{3-x}$ (a: x = 3; b: x = 2; c: x = 1; d: x=0) which were calculated via Eq. 1.

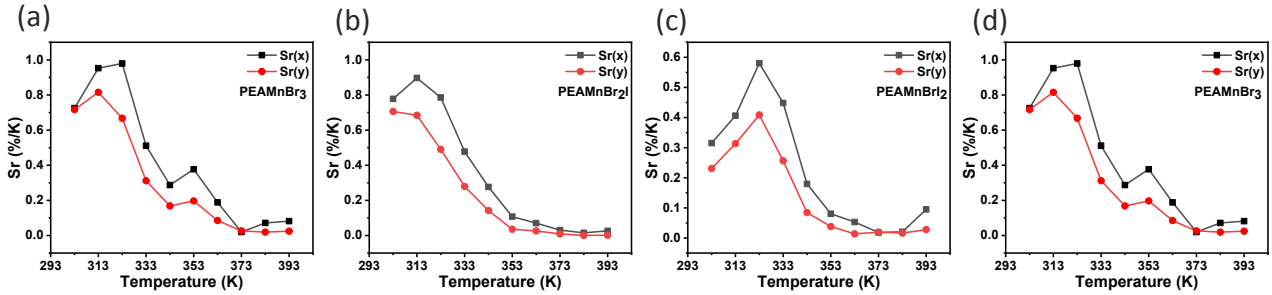


**Figure S18.** Thermal evolution of the relative sensitivity values of chromaticity coordinates x and y for $PEAMnBr_xI_{3-x}$ (a: x = 3; b: x = 2; c: x = 1; d: x=0).

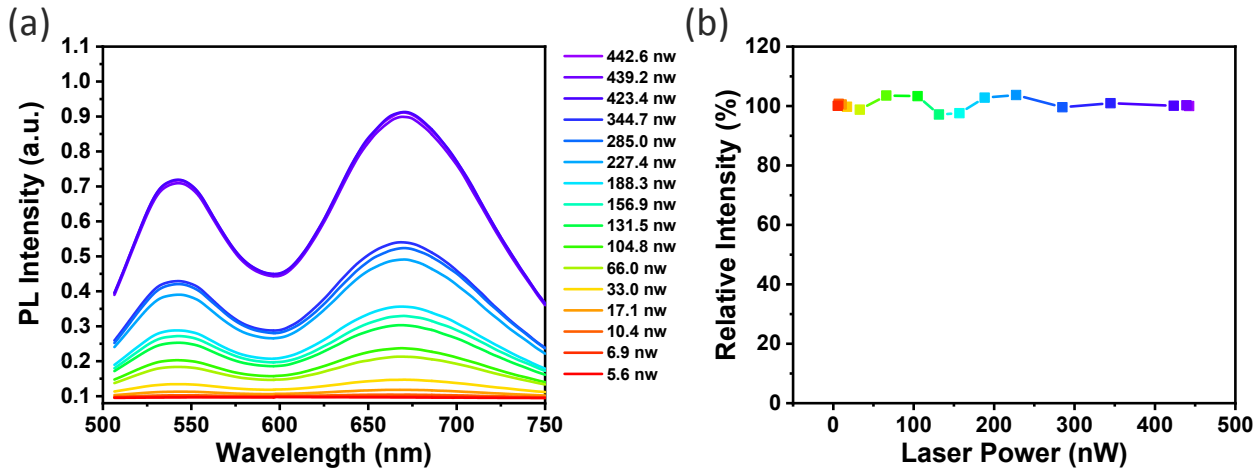


**Figure S19.** (a) Luminescence spectra of $PEAMnBr_2I$ corresponding to different power of 374 nm picosecond laser. (b) Relative luminescence intensities of $I_{540\ nm}/I_{660\ nm}$ exhibited lower than 3 % fluctuation corresponding to different power of 374 nm picosecond laser.

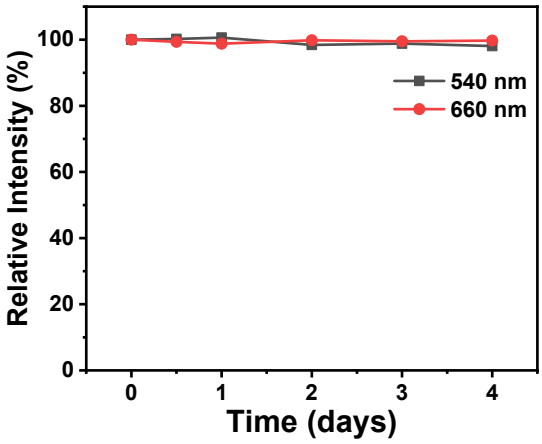


**Figure S20.** Relative intensity of $PEAMnBr_2I$ at 540 nm and 660 nm in different time of 365 nm UV irradiation (12 W). After 4-day continuous irradiation, the relative intensity exhibited lower than 1 % fluctuation.

***Additional Supporting Tables:***

**Table S1.** Comparison of the absolute and relative of sensitivities of diverse luminescent thermometers.

| Compound | $\lambda_{ex}$ | Temperature | $S_a$ | $S_r$ | Reference |
|---|---|---|---|---|---|
| $Er^{3+}$, $Yb^{3+}$: $LaF_3$ | 377.9 nm | 10 K – 105 K | / | 6.61 % $K^{-1}$ | 1 |
| $Ce^{3+}$, $Tb^{3+}$: β-$NaYF_4$ | 250 nm | 303 K – 563 K | 1.11 % $K^{-1}$ | 0.65 % $K^{-1}$ | 2 |
| $Mn^{2+}$, $Eu^{3+}$: $Zn2GeO_4$ | 315 nm | 293 K – 353 K | / | 1.96% $K^{-1}$ | 3 |
| Fluorescent Protein | 473 nm | 296 K – 313 K | / | / | 4 |
| C-dots | 400 nm | 288 K- 333 K | / | / | 5 |
| C-dots | 320 nm | 278 K- 358 K | 3.3 % $K^{-1}$ | / | 6 |
| Switchable Heterocycles | 415 nm | 281 K – 327 K | / | / | 7 |
| $BNMe_2$-BNaph | 340 nm | 253 K -353 K | 4.7 % $K^{-1}$ | / | 8 |
| Mn: $Cs_3Cu_2I_5$ | 300 nm | 298 K – 498 K | 54.7 % $K^{-1}$ | 0.525 % $K^{-1}$ | 9 |
| $PEAMnBr_3$ | 385 nm | 303 K – 393 K | 5.3 % $K^{-1}$ | / | This work |
| $PEAMnBr_2I$ | 385 nm | 303 K – 393 K | 37.0 % $K^{-1}$ | / | This work |
| $PEAMnBrI_2$ | 385 nm | 303 K – 393 K | 52.4 % $K^{-1}$ | / | This work |
| $PEAMnI_3$ | 385 nm | 303 K – 393 K | 58.0 % $K^{-1}$ | / | This work |

**Table S2.** Element contents from EDS mapping (according to Figure S1-S4).

| Samples | | Mn | Br | I |
|---|---|---|---|---|
| $PEAMnBr_3$ | 1 | 1 | 2.85 | 0 |
| | 2 | 1 | 2.71 | 0 |
| | 3 | 1 | 3.03 | 0 |
| | Average | 1 | 2.86 | 0 |
| $PEAMnBr_2I$ | 1 | 1 | 1.89 | 1.09 |
| | 2 | 1 | 1.89 | 1.09 |
| | 3 | 1 | 1.89 | 1.15 |
| | Average | 1 | 1.89 | 1.11 |
| $PEAMnBrI_2$ | 1 | 1 | 1.05 | 2.33 |
| | 2 | 1 | 0.98 | 1.96 |
| | 3 | 1 | 0.96 | 1.89 |
| | Average | 1 | 1 | 2.06 |
| $PEAMnBr_3$ | 1 | 1 | 0 | 2.78 |
| | 2 | 1 | 0 | 2.86 |
| | 3 | 1 | 0 | 2.94 |
| | Average | 1 | 0 | 2.86 |

**Table S3.** Element contents from XPS (according to Figure S6-S9).

| Samples | C% | N% | Mn% | Br% | I% |
|---|---|---|---|---|---|
| $PEAMnBr_3$ | 63.59 | 7.68 | 7.45 | 21.37 | 0 |
| $PEAMnBr_2I$ | 60.97 | 6.94 | 8.04 | 16.91 | 7.15 |
| $PEAMnBrI_2$ | 61.20 | 7.69 | 8.54 | 7.16 | 15.43 |
| $PEAMnI_3$ | 62.77 | 7.07 | 7.93 | 0 | 21.34 |

**Table S4.** CIE coordination of $PEAMnBr_xI_{3-x}$ (x = 0/1/2/3). Color temperatures were calculated according to $T_c = 437\times n^3+3601\times n^2+6831\times n+5517$, $n = (x-0.3320)/(0.1858-y)$.

| Samples | 30 °C | | 120 °C | |
|---|---|---|---|---|
| | x | y | x | y |
| $PEAMnBr_3$ | 0.5134 | 0.4660 | 0.3530 | 0.6047 |
| $PEAMnBr_2I$ | 0.4741 | 0.5046 | 0.3491 | 0.6175 |
| $PEAMnBrI_2$ | 0.4540 | 0.5324 | 0.3750 | 0.6008 |
| $PEAMnI_3$ | 0.3911 | 0.5907 | 0.3635 | 0.6138 |

**Table S5.** Lifetime data of $PEAMnBr_xI_{3-x}$ (x = 0/1/2/3) at room temperature and high temperature

| Composition | Temperature | Lifetime | | | | | | | |
|---|---|---|---|---|---|---|---|---|---|
| | | Room Temperature | | | | High Temperature | | | |
| | | $\tau_1$ (μs) | Percent % | $\tau_2$ (μs) | Percent % | $\tau_1$ (μs) | Percent % | $\tau_2$ (μs) | Percent % |
| $PEAMnBr_3$ | 545 nm | 66.41 | 65.97 | 3.04 | 34.03 | 82.67 | 82.67 | 2.58 | 17.33 |
| | 665 nm | 86.3 | 85.01 | 2.18 | 14.99 | 80.67 | 83.82 | 2.24 | 16.18 |
| $PEAMnBr_2I$ | 545 nm | 37.76 | 91.62 | 4.42 | 8.38 | 42.32 | 98.04 | 0.99 | 1.96 |
| | 665 nm | 35.28 | 77.97 | 1.39 | 22.03 | 35.31 | 75.12 | 1.55 | 24.88 |
| $PEAMnBrI_2$ | 545 nm | 26.75 | 92.95 | 3.37 | 7.05 | 31.04 | 100 | / | / |
| | 665 nm | 28.27 | 97.27 | 0.66 | 2.73 | 28.36 | 96.6 | 0.86 | 3.4 |
| $PEAMnI_3$ | 545 nm | 31.81 | 100 | / | / | 31.69 | 100 | / | / |
| | 665 nm | 27.61 | 100 | / | / | 26.87 | 100 | / | / |

***Reference:***


1. Kaczmarek, A. M.; Kaczmarek, M. K.; Van Deun, R., $Er^{3+}$-to-$Yb^{3+}$ and $Pr^{3+}$-to-$Yb^{3+}$ energy transfer for highly efficient near-infrared cryogenic optical temperature sensing. *Nanoscale* **2019,** *11*, 833-837.
2. Ding, M.; Lu, C.; Chen, L.; Ji, Z., $Ce^{3+}/Tb^{3+}$ co-doped β-$NaYF_4$ dual-emitting phosphors for self-referencing optical thermometry. *J. Alloys Compd.* **2018,** *763*, 85-93.
3. Yao, H.; Zhang, Y.; Xu, Y., Dopant concentration-dependent morphological evolution of $Zn_2GeO_4:Mn^{2+}/Eu^{3+}$ phosphor and optical temperature sensing performance. *J. Alloys Compd.* **2019,** *770*, 149-157.
4. Donner, J. S.; Thompson, S. A.; Kreuzer, M. P.; Baffou, G.; Quidant, R., Mapping Intracellular Temperature Using Green Fluorescent Protein. *Nano Lett.* **2012,** *12*, 2107-2111.
5. Wang, C.; Xu, Z.; Cheng, H.; Lin, H.; Humphrey, M. G.; Zhang, C., A hydrothermal route to water-stable luminescent carbon dots as nanosensors for pH and temperature. *Carbon* **2015,** *82*, 87-95.
6. Nguyen, V.; Yan, L.; Xu, H.; Yue, M., One-step synthesis of multi-emission carbon nanodots for ratiometric temperature sensing. *Appl. Surf. Sci.* **2018,** *427*, 1118-1123.
7. Mazza, M. M. A.; Cardano, F.; Cusido, J.; Baker, J. D.; Giordani, S.; Raymo, F. M., Ratiometric temperature sensing with fluorescent thermochromic switches. *Chem.Commun.* **2019,** *55*, 1112-1115.
8. Sun, Z. B.; Liu, J. K.; Yuan, D. F.; Zhao, Z. H.; Zhu, X. Z.; Liu, D. H.; Peng, Q.; Zhao, C. H., 2,2'-Diamino-6,6'-diboryl-1,1'-binaphthyl: A Versatile Building Block for Temperature-Dependent Dual Fluorescence and Switchable Circularly Polarized Luminescence. *Angew. Chem. Int. Ed.* **2019,** *58*, 4840-4846.
9. Du, P.; Cai, P.; Li, W.; Luo, L.; Hou, Y.; Liu, Z., Ratiometric optical thermometer based on the use of manganese(II)-doped $Cs_3Cu_2I_5$ thermochromic and fluorescent halides. *Microchimica Acta* **2019,** *186*.